Non-phase-matched optical third-harmonic generation in noncentrosymmetric media: Cascaded second-order contributions for the calibration of third-order nonlinearities

Christian Bosshard,* Ulrich Gubler, Phil Kaatz, Witold Mazerant, and Urs Meier
Nonlinear Optics Laboratory, Institute of Quantum Electronics, ETH Hönggerberg, CH-8093 Zürich, Switzerland
(Received 5 October 1999)

Cascaded second-order contributions to third-harmonic generation are analyzed in detail, and are exploited to obtain reliable reference values for third-order nonlinear optical susceptibilities at several wavelengths. We describe the influence of boundary conditions on the measured properties for the case of high nonlinearity crystals such as $KNbO_3$ and the organic salt 4-*N*, *N*-dimethylamino-4′-*N*′-methylstilbazolium toluene-*p*-sulfonate (DAST). Wavelength dispersion relations for the electronic third-order susceptibilities derived from third-harmonic generation experiments are discussed. Our reference standards allow a comparison of the third-harmonic generation results with measurements of the Kerr susceptibility determined with degenerate four-wave mixing and the *z*-scan technique and shows that $\chi^{(3)}(-\omega,\omega,-\omega,\omega) \geqslant \chi^{(3)}(-3\omega,\omega,\omega,\omega)$ in the investigated wavelength range. The investigation of structure-property relationships between the perovskite crystals $KNbO_3$ and $KTaO_3$ indicates similar bond nonlinearities in these two compounds.

I. INTRODUCTION

Third-order nonlinear optical effects are of prime importance for all-optical signal processing. In order to establish the usefulness of a material for these applications, the relevant nonlinearities have to be accurately known. Since the targeted effects should be very fast, electronic third-order processes are of great importance. The best technique of the investigation of these effects is third-harmonic generation, which allows one to probe electronic processes only. An often encountered problem with all nonlinear optical methods is, however, that the exact intensities of interacting optical waves are often not well known. For this reason most measurements are calibrated against a reference material with known nonlinearities. Therefore there exists a need for reliable reference materials. In this work we show that frequency tripling in combination with cascaded second-harmonic and sum-frequency generation is a very efficient tool to obtain self-consistent reliable reference values.

We present our experimental results on the crystals $KNbO_3$, $KTaO_3$, α-quartz, and 4-*N*, *N*-dimethylamino-4′-*N*′-methylstilbazolium toluene-*p*-sulfonate (DAST) and the glasses BK7, SF59, and fused silica with emphasis on the theoretical analysis of the cascaded phenomena including the boundary conditions, reliable reference materials, wavelength dispersion of the third-order susceptibilities, and structure-property relationships. In particular we want to address the following issues.

First, the calibration of third-order susceptibilities requires reliable values of second-order susceptibilities. The reference value of the second-order nonlinear optical susceptibilities $\chi^{(2)}$ of α-quartz has considerably changed over the last 15 years (from 1.0 pm/V down to 0.6 pm/V at $\lambda = 1064$ nm), and is now believed to be accurately known.[1,2] Kitamoto *et al.*[3] determined the nonlinear optical coefficient $\chi^{(2)}_{311} = 8.6 \pm 1.0$ pm/V of congruent $LiNbO_3$ with an absolute parametric fluorescence experiment at $\lambda = 532$ nm. A comparison with second-harmonic-generation experiments relative to α-quartz yielded a value for α-quartz of $\chi^{(2)}_{111} = 0.6$ pm/V. In a similar way the authors of Ref. 4 performed parametric fluorescence experiments with ADP($NH_4H_2PO_4$) (nonlinear optical coefficient $\chi^{(2)}_{312}$) at $\lambda = 632.8$ nm, which gave $\chi^{(2)}_{312} = 1.10 \pm 0.04$ pm/V. Phase-matched frequency-doubling experiments at $\lambda = 1064$ nm with ADP gave $\chi^{(2)}_{312} = 0.92 \pm 0.06$ pm/V, in perfect agreement with the value derived at this wavelength based on the Miller δ,[5]

$$\chi^{(2)}_{ijk}(-2\omega,\omega,\omega) = \frac{\chi_i^{2\omega}\chi_j^{\omega}\chi_k^{\omega}}{\chi_i^{2\omega'}\chi_j^{\omega'}\chi_k^{\omega'}}\chi^{(2)}_{ijk}(-2\omega',\omega',\omega') = \varepsilon_0\delta_{ijk}(\chi_i^{2\omega}\chi_j^{\omega}\chi_k^{\omega}), \quad (1)$$

which accurately describes the dispersion of second-order nonlinear optical susceptibilities in many inorganic materials. A subsequent Maker-fringe experiment with α-quartz as a reference at $\lambda = 1064$ nm yielded $\chi^{(2)}_{111} = 0.60 \pm 0.04$ pm/V. In addition, Maker-Fringe experiments at $\lambda = 632.8$ nm confirmed the validity of Miller's rule for ADP and α-quartz. Exact phase-matched frequency-doubling in bulk $KNbO_3$ crystals, and a comparison with Maker-Fringe experiments based on α-quartz also confirmed that $\chi^{(2)}_{111} = 0.60$ pm/V at $\lambda = 1064$ nm is a very realistic value.[6] This confirmed value can now be experimentally related to the electronic third-order susceptibilities through cascaded second-order nonlinear optical processes that yield the ratio $\chi^{(3)}/[\chi^{(2)}]^2$, as discussed below.

Second, the ratio of $\chi^{(3)}/[\chi^{(2)}]^2$, as obtained from third-harmonic generation experiments in noncentrosymmetric materials, is not very well determined for α-quartz, since its $\chi^{(2)}$ is rather small in comparison with its value for $\chi^{(3)}$. In contrast to quartz, high-quality crystals of $KNbO_3$ provide a much more favorable ratio of nonlinear susceptibilities. $KNbO_3$ has much larger nonlinear optical susceptibilities $\chi^{(2)}$ with respect to its $\chi^{(3)}$ values, and allows a more precise determination of the ratio $\chi^{(3)}/[\chi^{(2)}]^2$. We therefore performed our experiments with α-quartz and $KNbO_3$.

Third, the wavelength dependence of third-order susceptibilities of inorganic crystals is generally poorly understood. It is of fundamental interest also to establish a reliable standard for the dispersion of $\chi^{(3)}$, and to theoretically better understand the dispersion behavior. We show that a simple model based on a single oscillator adequately describes our experimental results.

Fourth, $KNbO_3$ was recently investigated for its third-order susceptibilities $\chi^{(3)}(-\omega,\omega,-\omega,\omega)$ by degenerate four-wave mixing[7,8] and the *z*-scan technique[9] using 100-ps laser pulses. A comparison between these measurements (where the third-order susceptibilities can contain electronic and optical-phonon contributions) and the third-harmonic experiments (only electronic contributions) described here will yield information of the importance of optical phonons for third-order nonlinear optics using inorganic crystals.

Fifth, the effect of longitudinal second-harmonic generation and boundary conditions on the third-harmonic signal is another relevant issue that may be important for high nonlinearity materials. The basic concept and its influence on α-quartz and $KNbO_3$ will be described below.

II. THEORY

A. Definition of nonlinear optical coefficients

For the definition of the nonlinear optical susceptibilities given below in Eq. (2), various conventions are frequently used. This has led to some confusion in the literature concerning the comparison of experimentally determined values obtained with different techniques. As an example, very often experimental values are directly compared to theoretical values that use a completely different convention. Moreover, most often the precise definitions in use are not clearly stated, which further complicates the comparison of nonlinear optical susceptibilities. Therefore we devote this section to a concise definition of the relevant processes.

The basic equation describing nonlinear optical effects expresses the macroscopic polarization P as a power series in the strength of the applied electric field E as

$$P_i = P_{0,i} + \varepsilon_0(\chi^{(1)}_{ij}E_j + \chi^{(2)}_{ijk}E_jE_k + \chi^{(3)}_{ijkl}E_jE_kE_l + \cdots), \tag{2}$$

where summation over common indices is understood. P_0 is the spontaneous polarization, $\chi^{(n)}$ is the nth-order susceptibility tensor, and ε_0 is the vacuum permittivity. The fundamental quantity describing second-order nonlinear optical effects is the tensor $\chi^{(2)}_{ijk}$. It is a third rank tensor which, in the electric dipole approximation, contains nonvanishing elements only for noncentrosymmetric molecular and crystalline structures.[10] Third-order nonlinearities are described through the tensor $\chi^{(3)}_{ijkl}$.

For the definition of the complex electric field amplitudes $E_n(\omega,k_n)$ we use the most widely applied convention

$$\mathbf{E}(\mathbf{r},t) = \tfrac{1}{2}\sum_n [\mathbf{E}_n(\omega,\mathbf{k}_n)\exp(i(\mathbf{k}_n\mathbf{r}-\omega t)) + \text{c.c.}]. \tag{3}$$

For the present discussion all quantities can be assumed to be real. Equations (2) and (3) then lead to the nonlinear polarizations relevant in this work ($P_i^{2\omega}$ for second-harmonic generation, $P_i^{\omega_3}$ for sum-frequency generation, and $P_i^{3\omega}$ for third-harmonic generation):

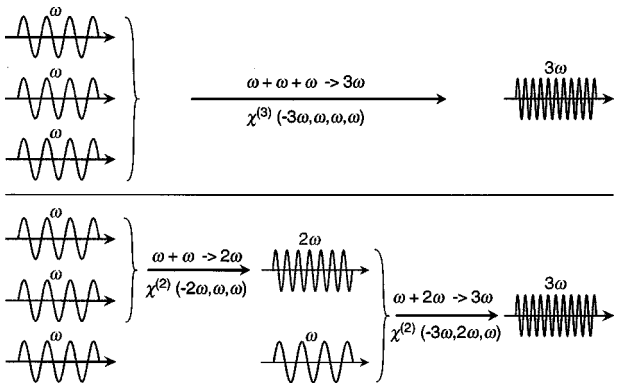

FIG. 1. Schematic of the generation of a wave at frequency 3ω through (a) direct third-harmonic generation ($\propto\chi^{(3)}(-3\omega,\omega,\omega,\omega)$) and (b) through cascaded second-harmonic and sum-frequency generation $[\propto\chi^{(2)}(-3\omega,2\omega,\omega)\times\chi^{(2)}(-2\omega,\omega,\omega)]$.

$$P_i^{2\omega} = \tfrac{1}{2}\varepsilon_0\chi^{(2)}_{ijk}(-2\omega,\omega,\omega)E_j^{\omega}E_k^{\omega} = \varepsilon_0 d^{(2)}_{ijk}(-2\omega,\omega,\omega)E_j^{\omega}E_k^{\omega}, \tag{4}$$

$$P_i^{\omega_3} = \varepsilon_0\chi^{(2)}_{ijk}(-\omega_3,\omega_1,\omega_2)E_j^{\omega_1}E_k^{\omega_2}, \tag{5}$$

$$P_i^{3\omega} = \tfrac{1}{4}\varepsilon_0\chi^{(3)}_{ijkl}(-3\omega,\omega,\omega,\omega)E_j^{\omega}E_k^{\omega}E_l^{\omega}. \tag{6}$$

d_{ijk} is the nonlinear optical coefficient for second-harmonic generation. Note that there is a prefactor that differs for sum-frequency generation and frequency doubling (a factor of 2 difference). This prefactor takes care that the low-frequency limit of all susceptibilities is the same for all frequency combinations.

B. Cascaded second-harmonic generation and sum-frequency generation

Cascading is a process where lower-order effects are combined to contribute to a higher-order nonlinear process. We illustrate this process for the case of third-harmonic generation (Fig. 1). Third-harmonic generation can occur in any material, even air (see below). In this process a fundamental wave at frequency ω produces a wave at frequency 3ω ($\omega+\omega+\omega=3\omega$). In noncentrosymmetric materials sum-frequency mixing ($\omega_1+\omega_2=\omega_3$) and second-harmonic generation ($\omega+\omega=2\omega$) are also allowed. We can use the two latter processes to also obtain a wave at frequency 3ω. We first generate an intermediate field at frequency 2ω through second-harmonic generation. This field can interact with the fundamental wave through sum-frequency mixing ($2\omega+\omega=3\omega$) to generate a field at frequency 3ω itself.[11,12] This combined process is called cascading, and is schematically illustrated in Fig. 1. To summarize: if we illuminate a noncentrosymmetric material with a wave at frequency ω and detect the third-harmonic wave (3ω) at the output, this output can contain two contributions: one from direct third-

harmonic generation [$\propto\chi^{(3)}(-3\omega,\omega,\omega,\omega)$], and one from cascaded second-harmonic generation and sum-frequency mixing [$\propto\chi^{(2)}(-3\omega,2\omega,\omega)\times\chi^{(2)}(-2\omega,\omega,\omega)$]. It is important to note that these intermediate fields do not need to be able to propagate. It is possible to generate longitudinal fields at frequency 2ω that can subsequently interact with photons at the fundamental frequency ω.

The cascading of second-order susceptibilities is also of great importance to all-optical signal processing. One of these cascaded effects which have been known for a long time leads to a nonlinear phase shift of the interacting waves in nearly phase-matched second-harmonic generation and other parametric processes.[13–17] Another interesting process contributing to cubic nonlinear effects comes from cascaded optical rectification and the linear electro-optic effect.[7–9,18,19]

Cascaded second-order processes allow the calibration of nonlinear optical susceptibilities without a knowledge of the laser parameters.[7,8,12,19] In the case of third-harmonic generation, this calibration can be described as follows: From a theoretical analysis of an experimental curve that shows cascaded processes one can directly obtain the ratio

$$\frac{\chi^{(3)}(-3\omega,\omega,\omega,\omega)}{\chi^{(2)}(-3\omega,2\omega,\omega)\times\chi^{(2)}(-2\omega,\omega,\omega)}. \tag{7}$$

Therefore, if the values of $\chi^{(2)}$ are known, the value of $\chi^{(3)}$ can be determined. This principle has been applied by Meredith[12] to find the values of $\chi^{(3)}$ of crystalline quartz (α-quartz) and fused silica, based on known values of $\chi^{(2)}$ of α-quartz. An advantage of cascaded second-harmonic and sum-frequency generation is the fact that only electronic effects are measured, this in contrast to, e.g., the *z*-scan technique[20] or degenerate four-wave mixing,[21] in which all effects that are fast enough (that can react within the duration of the pulses used in the experiment) can contribute (especially optical phonons). Note that similar calibration experiments were also applied to degenerate four-wave mixing.[8,19]

C. Boundary conditions

The local field can influence cascaded second-harmonic generation and sum-frequency generation in third-harmonic generation of noncentrosymmetric media.[11,12,22] We investigate this influence in a discussion that can be generalized to other cascaded processes.

In the case of second-harmonic generation in noncentrosymmetric materials, we have a source polarization $P_{\mathrm{NLS}}^{2\omega}$ (NLS is the nonlinear source) and a bound second-harmonic wave $E^{2\omega}$, to be inserted into the wave equation, that are related by (derived from the wave equation, neglecting wave vector and polarization dependencies)

$$E^{2\omega}=\frac{P_{\mathrm{NLS}}^{2\omega}}{\varepsilon_0(\varepsilon^{\omega}-\varepsilon^{2\omega})} \quad \text{(transverse case)}, \tag{8}$$

$$E^{2\omega}=-\frac{P_{\mathrm{NLS}}^{2\omega}}{\varepsilon_0\varepsilon^{2\omega}} \quad \text{(longitudinal case)}. \tag{9}$$

Each crystal lattice site (atom or molecule) experiences a local field described by[11]

$$E_L^{2\omega}=E^{2\omega}+L^{2\omega}P^{2\omega}+L^{2\omega}P_{\mathrm{NLS}}^{2\omega}=f^{2\omega}E^{2\omega}+L^{2\omega}P_{\mathrm{NLS}}^{2\omega}, \tag{10}$$

where $L^{2\omega}=1/(3\varepsilon_0)$, and $f^{2\omega}$ is the local-field factor given by $[(n^{2\omega})^2+2]/3$ in the Lorentz approximation. Note that Eq. (10) differs from the usual linear case

$$E_L^{\omega}=E^{\omega}+L^{\omega}P^{\omega}=f^{\omega}E^{\omega}. \tag{11}$$

Equation (10) can be further changed to

$$E_L^{2\omega}=f^{2\omega}\left\{E^{2\omega}+\frac{L^{2\omega}}{f^{2\omega}}P_{\mathrm{NLS}}^{2\omega}\right\}\equiv f^{2\omega}E_{\mathrm{eff}}^{2\omega}, \tag{12}$$

where $E_{\mathrm{eff}}^{2\omega}$ is the effective field that has to be applied when deriving $P_{\mathrm{NLS}}^{2\omega}$ from macroscopic fields. $E_{\mathrm{eff}}^{2\omega}$ should only be applied for the generation of $P^{3\omega}$ (the bound wave for second-harmonic generation remains unchanged). In the Lorentz approximation, $E_{\mathrm{eff}}^{2\omega}$ becomes

$$E_{\mathrm{eff}}^{2\omega}=\left\{\frac{1}{\varepsilon^{\omega}-\varepsilon^{2\omega}}+\frac{1}{\varepsilon^{2\omega}+2}\right\}\frac{P_{\mathrm{NLS}}^{2\omega}}{\varepsilon_0} \quad \text{(transverse case)}, \tag{13}$$

$$E_{\mathrm{eff}}^{2\omega}=\left\{-\frac{1}{\varepsilon^{2\omega}}+\frac{1}{\varepsilon^{2\omega}+2}\right\}\frac{P_{\mathrm{NLS}}^{2\omega}}{\varepsilon_0} \quad \text{(logitudinal case)}. \tag{14}$$

The second term in $E_{\mathrm{eff}}^{2\omega}$ leads to a modification of the effective third-order nonlinear optical susceptibility (in addition to the ''usual'' cascading). This effect was called *cascading through the local field* by Meredith.[12] We prefer to view this effect as a result of the electromagnetic boundary conditions. In the case of transverse fields the modified third-order nonlinear optical susceptibility is then

$$\chi_{\mathrm{eff}}^{3\omega}=\chi^{3\omega}+2\chi_{\mathrm{SHG}}^{2\omega}\times\chi_{\mathrm{SFG}}^{3\omega}\left\{\frac{1}{\varepsilon^{\omega}-\varepsilon^{2\omega}}+\frac{1}{\varepsilon^{2\omega}+2}\right\}, \tag{15}$$

where SHG and SFG refer to second-harmonic generation and sum-frequency generation, respectively. In the case of phase-matched interactions $\varepsilon^{\omega}\approx\varepsilon^{2\omega}$, the term

$$\frac{L^{2\omega}}{f^{2\omega}}P_{\mathrm{NLS}}^{2\omega} \tag{16}$$

can be neglected in a first approximation. For longitudinal fields, we obtain

$$\chi_{\mathrm{eff}}^{3\omega}=\chi^{3\omega}+2\chi_{\mathrm{SHG}}^{2\omega}\times\chi_{\mathrm{SFG}}^{3\omega}\left\{-\frac{1}{\varepsilon^{2\omega}}+\frac{1}{\varepsilon^{2\omega}+2}\right\} \tag{17}$$

D. Wavelength dependence of second- and third-order susceptibilities of inorganic materials

For second-order nonlinear optics (second-harmonic and sum-frequency generation), Eq. (1) accurately describes the dispersion of second-order nonlinear optical susceptibilities in many inorganic materials with wavelength-independent Miller δ coefficients. However, we found (see below) that this simple relation does not hold for the case of $KNbO_3$. An appropriate equation describing our results for this case is based on the model of a single oscillator, and is given by

$$\chi^{(2)}_{iii}(-\omega_3,\omega_2,\omega_1)=\varepsilon_0\frac{\delta_{iii}}{(\omega_0^2-\omega_1^2)(\omega_0^2-\omega_2^2)(\omega_0^2-\omega_3^2)}-\mathcal{I}\times(\lambda_1^2+\lambda_2^2+\lambda_3^2) \quad (18)$$

for sum-frequency generation. The last term of this equation takes into account contributions from lattice oscillations in the infrared and is described by the parameter $\mathcal{I}$.

For third-harmonic generation, useful theoretical descriptions have been discussed for quite some time, since it is of fundamental interest to know the dispersion of $\chi^{(3)}$ for at least two reasons; (i) to obtain a better theoretical understanding of the dispersion behavior in inorganic (and organic) materials: and (ii) to obtain a reliable standard for the wavelength dependence of $\chi^{(3)}$. A generalization of Miller's rule [Eq. (1)] to third-order nonlinearities,[23]

$$\chi^{(3)}_{ijkl}(-3\omega,\omega,\omega,\omega)=\varepsilon_0\delta_{ijkl}(\chi_i^{3\omega}\chi_j^{\omega}\chi_k^{\omega}\chi_l^{\omega}), \quad (19)$$

has not been as successful in predicting the wavelength dispersion as in second-order nonlinear optics. Wang[24] proposed a different relationship that seems to be more generally valid. In the limit $\omega->0$ he obtained

$$\chi^{(3)}_{iiii}=Q[\chi_i^{(1)}]^2, \quad (20)$$

A further treatment by Boling, Glass, and Owyoung[25] yielded

$$\chi^{(3)}_{iiii}=Q'[n_i^2+2]^2[n_i^2-2], \quad (21)$$

where Q and Q' are quantities that are wavelength independent for many materials. A further approach is based on the simple model of a single electronic oscillator as in the case of $KNbO_3$ for sum-frequency generation.[26] As we concentrate on the transparent spectral region of our materials, we neglected possible two-photon resonances in the first approximation. In this case the dispersion of the third-order susceptibility for third-harmonic generation is described by

$$\chi^{(3)}_{iiii}(-3\omega,\omega,\omega,\omega)=\varepsilon_0\frac{\delta_{iiii}}{(\omega_0^2-\omega^2)^3(\omega_0^2-(3\omega)^2)}. \quad (22)$$

It should be noted that in contrast to the other equations the relation in Eq. (22) contains two adjustable parameters. We will discuss these dispersion relations for the cases of fused silica, α-quartz, BK7, and $KNbO_3$ and show that Eq. (22) best describes our experimental results.

III. MATERIALS DESCRIPTION

In the following, we briefly describe the most important parameters required for our experiments. We investigated the fused silica, glasses BK7, and SF59, and the crystals α-quartz (point group 32), $KNbO_3$ (point group $mm2$), $KTaO_3$ (point group $m3m$), and the organic salt 4-N,N-dimethylamino-4′-N′-methylstilbazolium toluene-p-sulfonate (DAST) (point group m). Fused silica and BK7 are often used as reference materials in third-order nonlinear optical experiments. SF59 is a glass with a large refractive index and enhanced third-order nonlinearities with respect to fused silica.[27,28] We investigated it since it could very well serve as a reference material with a large third-order nonlinear optical response. α-quartz is a well characterized trigonal crystal that is mainly used as a standard reference material both for $\chi^{(2)}$ and $\chi^{(3)}$.

$KNbO_3$ and $KTaO_3$ are both perovskite (ABO_3) compounds. Whereas $KTaO_3$ has cubic symmetry at room temperature,[29] $KNbO_3$ is only cubic at high temperatures, and transforms with decreasing temperature to the tetragonal (at $\sim$440 °C), orthorhombic (at 223 °C) and rhombohedral (at -50 °C) phases.[30] In a first approximation we can assume that the cubic contributions to $\chi^{(3)}$ are the same for $KTaO_3$ and $KNbO_3$. A comparison of the experimental electronic nonlinear optical susceptibilities of the two will show whether our assumption is justified.

DAST consists of a typical donor-acceptor π-conjugated molecule, and a guest molecule that form high-quality noncentrosymmetric crystals with large second-order nonlinearities.[31] In DAST crystals the angular deviation of the charge-transfer axes of the stilbazolium chromophores from a completely aligned system is about 20°,[32] which gives rise to exceptionally large second-order susceptibilities. Also, large third-order susceptibilities are expected for light polarized along the polar axis a. Since DAST has very large second-order nonlinear optical susceptibilities (e.g., $\chi^{(2)}_{111}=2020\pm220$ pm/V at $\lambda=1318$ nm), significant cascaded second-order effects are expected as well.[19]

IV. FREQUENCY CONVERSION EXPERIMENTS

A. Second-harmonic generation

Most of the results described here rely on the nonlinear susceptibility $\chi^{(2)}_{111}=0.60$ pm/V of α-quartz at $\lambda=1064$ nm. Since the cascaded contributions to third-harmonic generation are not very pronounced for this material, $KNbO_3$ was additionally used whenever possible. In order to obtain reliable values we first always measured the relevant nonlinear optical coefficient $\chi^{(2)}_{333}$ of $KNbO_3$ with respect to $\chi^{(2)}_{111}$ of α-quartz [assuming that the Miller δ with

$$\delta_{111}=(2.66\pm0.09)\times10^{-2}\ \mathrm{m^2/C}$$

for α-quartz holds up to a wavelength of 2100 nm] with frequency doubling, and subsequently analyzed the same crystals with third-harmonic generation.

Several pulsed nanosecond laser sources were used for the second-harmonic generation experiments. A Nd:YAG (yttrium aluminum garnet) laser ($\lambda=1.064\ \mu$m, a 10-Hz repetition rate, and a pulse duration of 5 ns) either directly generated the second-harmonic or pumped a H_2 gas Raman cell, yielding a frequency shifted wavelength of 1.907 μm. In addition a Nd:YAG laser ($\lambda=1.318\ \mu$m, a 10-Hz repetition rate, and a pulse duration of 60 ns) and a HoTmCr:YAG laser ($\lambda=2.1\ \mu$m, a 2-Hz repetition rate, and a pulse duration of 80 ns) were used. The fundamental beam was then focused onto the sample with a $f=500$ mm lens, and the generated second-harmonic wave was detected with a photomultiplier. The beams at frequencies ω and 2ω were always s polarized. The second-harmonic-generation measurements were performed by rotating the samples around an axis parallel to the polarization to generate well-known Maker-fringe interference patterns. Figure 2 shows the experimental setup used. As in usual nonlinear optical experiments, the Maker-fringe curves were referenced against a well-known material

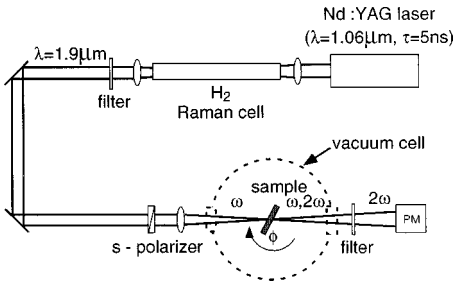

FIG. 2. Experimental setup for second- and third-harmonic generation for a fundamental wave at $\lambda = 1907$ nm. Here the case of second-harmonic generation is shown. The *s*-polarized fundamental is focused on the sample. The generated light at 2ω or 3ω is incident on a photomultiplier tube. Filters are used to reject the fundamental beam and to keep the signal within the linear range of the detection setup. In the case of third-harmonic generation, the sample is kept in a vacuum chamber with glass windows (dashed line) to exclude contributions from air.

which in our case was α-quartz. We measured the nonlinear optical susceptibility $\chi^{(2)}_{333}$ of $KNbO_3$ at the four wavelengths mentioned above. The theoretical analysis of the experimental Maker-fringe curves was based on the equations of Ref. 33.

B. Third-harmonic generation

The same laser sources as in the case of the second-harmonic-generation experiments were used. Third-harmonic-generation measurements were performed by rotating the samples around an axis parallel to the polarization to generate well-known Maker-fringe interference patterns. The beams at frequency ω and 3ω were always *s* polarized. Figure 2 shows the experimental setup used. All measurements were either carried out in vacuum except for DAST which was measured in air according to a specially developed procedure.[34] It is important to realize that reliable measurements have to be carried out in vacuum (in our case we used 0.05–0.1 bar) because air also makes an important contribution to the third-harmonic signal. The reason for this arises from the large coherence length of air, $l_c = \lambda/[6(n^{3\omega} - n^{\omega})]$, due to an almost dispersionless refractive index, and the fact that the signal at the third-harmonic is proportional to the product $[\chi^{(3)}]^2 l_c^2$. The materials of interest have a large value of $\chi^{(3)}$, but a small coherence length of the order of 10–100 μm, whereas air, on the other hand, has a very small value of $\chi^{(3)}$ but a very large coherence length (e.g., $l_c = 1.5$ cm at $\lambda = 1000$ nm, the refractive index data taken from Ref. 35).

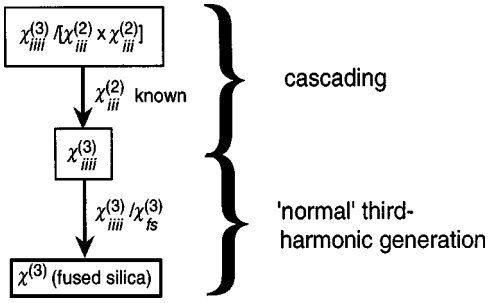

FIG. 3. Schematic diagram of the procedure to determine the third-order nonlinearity of fused silica based on the cascading of second-order nonlinearities in third-harmonic generation.

TABLE I. Second-order susceptibilities of α-quartz ($\chi^{(2)}_{111}$ and $[\chi^{(2)}_{111}]^2$) and $KNbO_3$ ($\chi^{(2)}_{333}$ and $[\chi^{(2)}_{333}]^2$). $[\chi^{(2)}]^2$ is equal to $\chi^{(2)}(-3\omega,2\omega,\omega)\times\chi^{(2)}(-2\omega,\omega,\omega)$. $\chi^{(2)}(-2\omega,\omega,\omega)$ and $\chi^{(2)}(-3\omega,2\omega,\omega)$ were calculated from Eq. (1) (for α-quartz) and Eq. (18) (for $KNbO_3$).

λ (nm)	$\chi^{(2)}_{111}(-2\omega,\omega,\omega)$ (pm/V)	$[\chi^{(2)}_{111}]^2$ $(pm/V)^2$	$\chi^{(2)}_{333}(-2\omega,\omega,\omega)$ (pm/V)	$[\chi^{(2)}_{333}]^2$ $(pm/V)^2$
		α-quartz		$KNbO_3$
1064	0.600±0.040	0.385	44.2±1.2	-
1318	0.584±0.040	0.359	40.6±1.0	1940
1907	0.555±0.040	0.322	33.2±1.2	1330
2100	0.545±0.040	0.312	31.2±1.2	1170

Different geometrical conditions were selected in order to distinguish between cascaded second-harmonic and sum-frequency generation and pure third-harmonic generation. At 2100 nm, 1907 nm and 1318 nm measurements were performed with α-quartz and $KNbO_3$. At $\lambda = 1064$ nm only α-quartz was investigated, since the third harmonic was absorbed in $KNbO_3$ too strongly. The data points for angles of incidence between $-5°$ and $+5°$ were always neglected due to clearly visible multiple reflections that can influence the results. The same samples of α-quartz and $KNbO_3$ were used for second- and third-harmonic generation. All third-harmonic-generation experiments were also referenced to fused silica to establish a reliable reference value for that material (see Sec. IV).

The equations for the theoretical analysis can be found in the Appendix. We extended our theory from that of Ref. 12 in that we treat rotational Maker fringes, and include the contributions from air. Reference 4 also treated rotational Maker fringes (without air contributions), but had a different (wrong) sign in their Eq. (31).

C. Absolute value of the third-order susceptibilities

As mentioned above, a special feature of cascading is the fact that it often is a self-calibrating process.[8,12,19] In the case

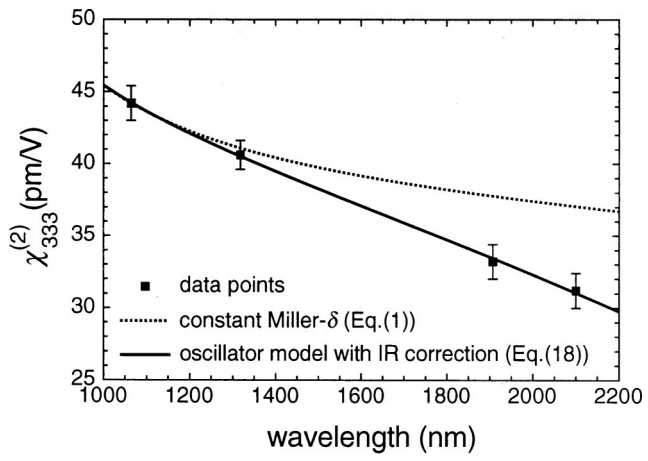

FIG. 4. Dispersion of the second-order susceptibility $\chi^{(2)}_{333}$ of $KNbO_3$ with two theoretical models. It is clearly seen that the Miller δ poorly describes the dispersion.

TABLE II. Ratios $\chi^{(3)}/(\chi^{(2)})^2$ for α-quartz ($\chi^{(3)}_{1111}/[\chi^{(2)}_{111}]^2$) and $KNbO_3$($\chi^{(3)}_{3333}/[\chi^{(2)}_{333}]^2$) obtained from third-harmonic-generation experiments with (#) and without contributions from the boundary conditions. \$ indicates the data after weighted averaging. It should be noted that $\chi^{(3)}/(\chi^{(2)})^2(\mathrm{SI})=(1/4\pi)\chi^{(3)}/(\chi^{(2)})^2$ (esu).

λ (nm)	$\chi^{(3)}/(\chi^{(2)})^2$ α-quartz	$\chi^{(3)}/(\chi^{(2)})^{2\#}$ α-quartz	$\chi^{(3)}/(\chi^{(2)})^{2\#,\$}$ α-quartz	$\chi^{(3)}/(\chi^{(2)})^2$ $KNbO_3$	$\chi^{(3)}/(\chi^{(2)})^{2\#}$ $KNbO_3$	$\chi^{(3)}/(\chi^{(2)})^{2\#,\$}$ $KNbO_3$
1064	643±40	643±40	643	-	-	-
1318	608±41	608±41	616	3.50±0.13	3.20±0.13	3.18
1907	588±35	588±35	618	3.89±0.08	3.58±0.08	3.58
2100	850±260	850±260	663	3.53±0.11	3.22±0.08	3.22

of cascading in third-harmonic generation this means that a theoretical fit of an experimental curve that shows cascaded processes directly yields the ratio $\chi^{(3)}/(\chi^{(2)})^2$ without any required knowledge of the laser beam parameters. Therefore, if the values of $\chi^{(2)}$ are known, the value of $\chi^{(3)}$ can be determined. A reference measurement with, e.g., fused silica, then yields a value of $\chi^{(3)}$ for that material (Fig. 3). This principle was applied by Meredith[12] to find the values of $\chi^{(3)}$ of crystalline quartz (α-quartz) and fused silica based on known values of $\chi^{(2)}$ of α-quartz. We here extend the work to different wavelengths, additional materials to obtain better ratios $\chi^{(3)}/(\chi^{(2)})^2$, and by applying the rotational Maker-fringe technique.

V. RESULTS

A. Second-harmonic generation

If accurate values should be obtained the influence of multiple reflections on the generated harmonic signals have to be considered. We investigated the cases of coherent and incoherent multiple reflections.[36] A careful evaluation of different parts of the Maker-fringe curves always yielded the same results for the third-order susceptibilities, and therefore indicated that coherent multiple reflections can be neglected. For the case of incoherent contributions where we sum over all reflections from the two sample surfaces we obtained a reduction of $\chi^{(2)}_{333}$ for $KNbO_3$ of 1% when taking these reflections into account by

$$\chi^{(2)\prime}_{333}=\chi^{(2)}_{333}\times\frac{[1-(r^{2\omega})^4][1-(r^{\omega})^8]}{1+(r^{2\omega})^2(r^{\omega})^4}, \qquad (23)$$

where r^{ω} is the Fresnel reflection coefficient given by $r^{\omega}=(n^{\omega}-1)^2/(n^{\omega}+1)^2$. Our experimental results for the nonlinear optical susceptibility $\chi^{(2)}_{333}$ of $KNbO_3$ [including the correction of Eq. (23)] are given in Table I, and displayed in Fig. 4. The theoretical curve in Fig. 4 is based on Eq. (18), and was subsequently used for a calculation of the relevant nonlinear optical susceptibilities $[\chi^{(2)}]^2$ for the cascading experiments. It is clearly seen that the curve based on the Miller δ does not adequately describe the dispersion of the $\chi^{(2)}_{333}$ of $KNbO_3$, in contrast to the oscillator model with an infrared correction term. Therefore it is also of no surprise that the Miller δ does not describe the dispersion of the third-order susceptibility either, as will be shown below.

B. Cascaded second-harmonic generation and sum-frequency generation

The second-order nonlinear optical susceptibilities $\chi^{(2)}$ of α-quartz and $KNbO_3$ at different wavelengths were obtained as just described. $\chi^{(2)}(-2\omega,\omega,\omega)$ and $\chi^{(2)}(-3\omega,2\omega,\omega)$ were calculated from Eq. (1) (for α-quartz) and Eq. (18) (for $KNbO_3$). The experimental results were subsequently used in the evaluation of the third-harmonic generation experiments that we carried out as described above.

In analogy to frequency doubling, incoherent multiple reflections were also taken into account for third-harmonic generation. This leads to modified third-order nonlinear optical susceptibilities

$$\chi^{(3)\prime}=\chi^{(3)}\times\frac{[1-(r^{3\omega})^4][1-(r^{\omega})^{12}]}{1+(r^{3\omega})^2(r^{\omega})^6}. \qquad (24)$$

These corrections do not influence the ratio $\chi^{(3)}/[\chi^{(2)}]^2$, but modify the third-order susceptibilities by 1–2 % for materi-

TABLE III. New absolute values of $\chi^{(3)}$ (in units of $10^{-22}\,\mathrm{m^2/V^3}$) based on third-harmonic-generation experiments of α-quartz and $KNbO_3$ with (#) and without contributions from the boundary conditions. For the derivation of these values we assumed the second-order susceptibilities of α-quartz and $KNbO_3$ to be exact. If, additionally, errors for them are introduced, the uncertainties for the values given below become approximately twice as large.

λ (nm)	$\chi^{(3)}_{1111}$ α-quartz	$\chi^{(3)}_{3333}$ $KNbO_3$	$\chi^{(3)}_{fs}$	$\chi^{(3)}_{1111}$# α-quartz	$\chi^{(3)}_{3333}$# $KNbO_3$	$\chi^{(3)}_{fs}$#
1064	2.48±0.15	-	1.99±0.15	2.48±0.15	-	1.99±0.15
1318	2.21±0.12	67.5±2.5	-	2.21±0.12	61.7±2.5	-
1907	1.99±0.08	51.5±1.1	1.62±0.06	1.99±0.08	47.4±1.1	1.62±0.06
2100	2.06±0.12	41.3±1.3	1.63±0.11	2.06±0.13	37.7±1.3	1.63±0.11

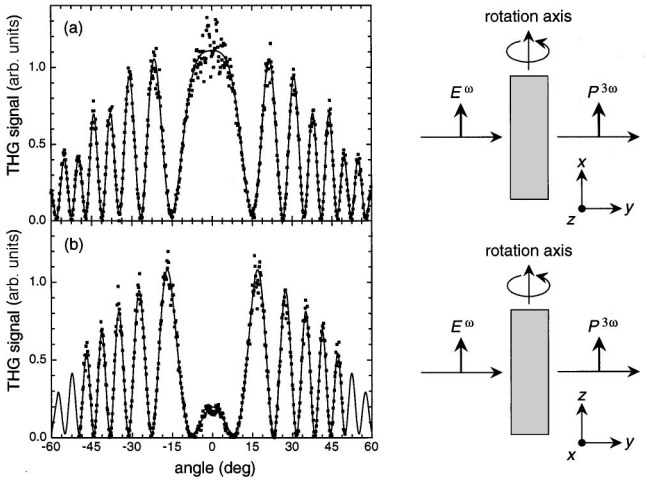

FIG. 5. Third-harmonic Maker-fringe curves of a *y* plate of α-quartz at $\lambda = 1907$ nm. (a) Light polarizations along *x* where cascaded second-order contributions appear. The interference effects are not very pronounced since the value of $\chi^{(2)}$ is quite small as compared to $\chi^{(3)}$. (b) Light polarizations along *z* where no cascaded second-order contributions are present.

als with large refractive indices, $KNbO_3$, $KTaO_3$, and SF59. The influence of the boundary conditions will be discussed separately (Sec. VI).

For the determination of absolute values for $\chi^{(3)}$ the ratios $\chi^{(3)}_{iiii}/[\chi^{(2)}_{iii}]^2$ and $\chi^{(3)}_{iiii}/\chi^{(3)}_{fs}$ were first obtained from the experimental Maker-fringe curves (Table II). The first ratio yields $\chi^{(3)}_{iiii}$ based on the known value of $\chi^{(2)}_{iii}$. From the second ratio $\chi^{(3)}_{fs}$ can subsequently be determined (Fig. 3). This procedure was carried out for α-quartz and $KNbO_3$. The results, weighted with the experimental errors, are summarized in Table III. The final values are the ones including the boundary conditions. Inclusion of this effect hardly influences the values for α-quartz and fused silica. Only in the case of $KNbO_3$ can a reduction in the values of $\chi^{(3)}$ be noted (Table III).

For α-quartz, *x* and *y* plates were investigated (Fig. 5). From symmetry considerations we have $\chi^{(3)}_{1111}(-3\omega,\omega,\omega,\omega)=\chi^{(3)}_{2222}(-3\omega,\omega,\omega,\omega)$. The *x* and *y* plates were rotated with their axes along the crystallographic *y* and *z* axes (the *x* plate) and *x* and *z* axes (the *y* plate, Fig. 5). Only for the *y* plate with rotation axis and light polarizations along the *x* axis is cascading observed $[\chi^{(2)}_{111}(-3\omega,2\omega,\omega)\times\chi^{(2)}_{111}(-2\omega,\omega,\omega)]$. For light polarized along the *z* axis (both *x* and *y* plates), only the interaction with $\chi^{(3)}_{3333}(-3\omega,\omega,\omega,\omega)$ produces a third-harmonic signal.

From a measurement of the *x* plate with the rotation axis and light polarizations along the *y* axis we expect the same value of $\chi^{(3)}$ as for the first configuration (a *y* plate with a rotation axis and light polarizations along *z*) due to symmetry considerations. Our experimental results are summarized in Tables III and IV.

In $KNbO_3$, *a*, *b*, and *c* plates were investigated. To determine the cascaded contributions the *a* and *b* plates were rotated around the crystallographic *c* direction, and the polarizer and analyzer were chosen along the same direction. This yields a signal at the third-harmonic wavelength that depends on $\chi^{(3)}_{3333}(-3\omega,\omega,\omega,\omega)$ and

$$\chi^{(2)}_{333}(-3\omega,2\omega,\omega)\times\chi^{(2)}_{333}(-2\omega,\omega,\omega).$$

TABLE IV. Summary of all third-harmonic-generation experiments $\chi^{(3)}$ (in units of 10^{-22} m^2/V^2) with (#) and without contributions from the boundary conditions.

Material	λ (nm)	$\chi^{(3)}_{1111}$	$\chi^{(3)}_{2222}$	$\chi^{(3)}_{3333}$	$\chi^{(3)}_{1133}$
α-quartz	1064	2.48±0.15	2.48±0.15	2.57±0.24	-
	1318	2.21±0.15	2.21±0.15	-	-
	1907	1.99±0.08	1.99±0.08	2.12±0.11	-
	2100	2.06±0.12	2.06±0.12	2.17±0.14	-
$KNbO_3$	1318	-	-	67.5±2.5	-
		-	-	61.7±2.5#	-
	1907	44±3	106±8	51.5±1.1	-
		44±3	106±8	47.4±1.1#	-
	2100	-	-	41.3±1.3	-
		-	-	37.7±1.3#	-
$KTaO_3$	1907	67±4	67±4	67±4	12.8±2.3 ($\chi^{(3)}_{\text{eff}}$=53±3)
SF59	1907	39.6±0.5	39.6±0.5	39.6±0.5	-
	2100	35.8±2.4	35.8±2.4	35.8±2.4	-
BK7	1064	2.98±0.26	2.98±0.26	2.98±0.26	-
	1907	2.38±0.11	2.38±0.11	2.38±0.11	-
	2100	2.29±0.16	2.29±0.16	2.29±0.16	-
fused silica	1064	1.99±0.15	1.99±0.15	1.99±0.15	-
	1907	1.62±0.06	1.62±0.06	1.62±0.06	-
	2100	1.63±0.11	1.63±0.11	1.63±0.11	-

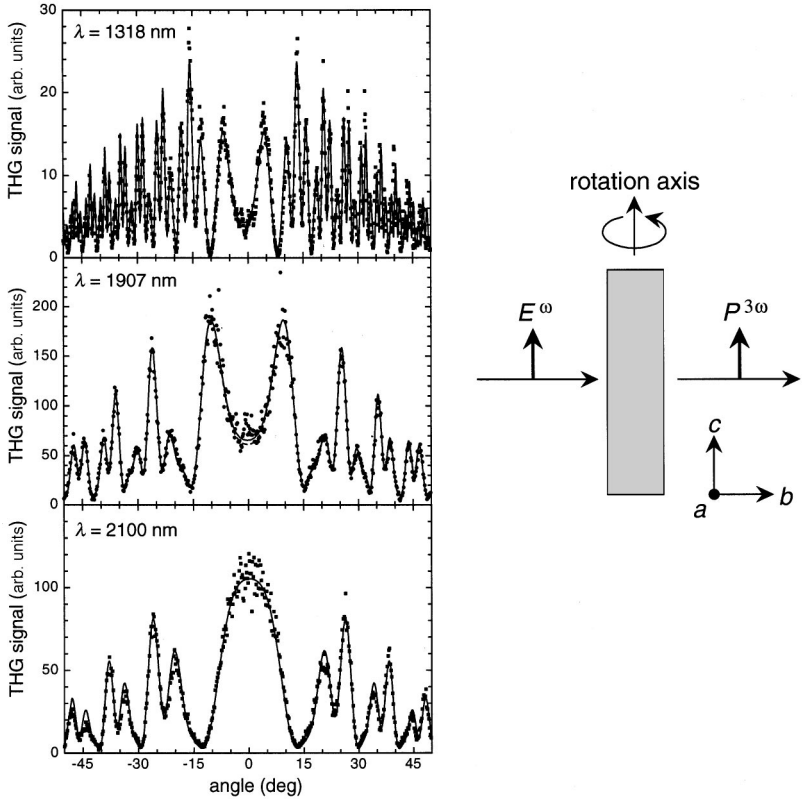

FIG. 6. Third-harmonic Maker-fringe curves of a *b* plate of $KNbO_3$ at three different wavelengths with clearly visible cascaded contributions. To the right the sample geometry is shown.

Figure 6 shows Maker-fringe curves of the same $KNbO_3$ crystal for three different wavelengths. It is nicely seen that increased dispersion leads to more complex interference patterns as the fundamental wavelength decreases. Results of these experiments for several *a* and *b* plates are summarized in Tables III and IV.

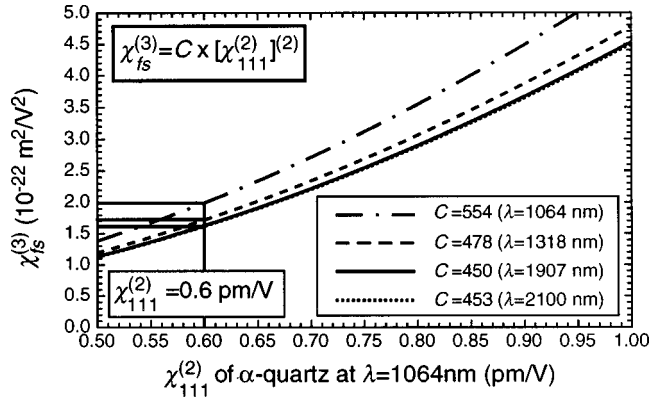

FIG. 7. Third-order nonlinear optical susceptibility $\chi^{(3)}(-3\omega,\omega,\omega,\omega)$ of fused silica at various wavelengths obtained from cascaded second-order processes in third-harmonic generation in α-quartz and $KNbO_3$ as a function of $\chi^{(2)}_{111}$ of α-quartz at $\lambda = 1064$ nm $\chi^{(3)}(\mathrm{SI})=[4\pi/9\times10^8]\times\chi^{(3)}(\mathrm{esu})$; SI:système internationale. The factor *C* contains the wavelength dispersion of $\chi^{(2)}_{111}$ of α-quartz based on the Miller δ. To derive $\chi^{(3)}_{\mathrm{fs}}$ of fused silica at any of the four indicated wavelengths from our measurements using a different value $\chi^{(2)}_{111}$ of α-quartz at $\lambda = 1064$ nm one just needs to insert that value into the appropriate equation to obtain the desired value of $\chi^{(2)}_{111}$. An example: if we had performed our evaluation based on $\chi^{(2)}_{111}=0.70$ pm/V, we would have obtained a value of $\chi^{(3)}_{\mathrm{fs}}=2.21\times10^{-22}\,\mathrm{m^2/V^2}$ at $\lambda = 1907$ nm.

Many experiments over the last years suggest that the value of the second-order susceptibility of α-quartz at $\lambda = 1064$ nm is $\chi^{(2)}_{111}=0.6$ pm/V. Nevertheless we show $\chi^{(3)}_{fs}$, based on our experiments, as a function of the square of $\chi^{(2)}_{111}$ of α-quartz at $\lambda = 1064$ nm in Fig. 7. The factor *C* contains the wavelength dispersion of $\chi^{(2)}_{111}$ of α-quartz for second-harmonic generation and sum-frequency generation based on the Miller δ [Eq. (1)]. The equation in Fig. 7 allows one to calculate the value of $\chi^{(3)}_{fs}$ at any of the wavelengths discussed in this work for any desired value of $\chi^{(2)}_{111}$ of α-quartz at $\lambda = 1064$ nm.

Typically third-harmonic Maker-fringe curves based on a combination of $\chi^{(3)}$ and $[\chi^{(2)}]^2$ show additional oscillations as compared to ''pure'' third-harmonic-generation curves (see Figs. 5 and 6). It is, however, possible to have cascaded contributions to third-harmonic generation that do not show additional oscillations, as illustrated in Fig. 8(a). This figure shows the example of a *b* plate of $KNbO_3$ with light polarized along *a*. In this geometry we have cascaded contributions through $\chi^{(2)}_{131}(-3\omega,2\omega,\omega)\times\chi^{(2)}_{311}(-2\omega,\omega,\omega)$. In our experiments these contributions could not be observed, since the relevant coherence lengths $[l_c(-3\omega,\omega,\omega,\omega) = 3.409\ \mu\mathrm{m}$ and $l_c(-3\omega,2\omega,\omega)=3.871\ \mu\mathrm{m}$ for perpendicular incidence] do not differ sufficiently. A theoretical analysis of the curve without cascading in Fig. 8(a) yields values of $\chi^{(3)}_{1111}$ that are typically 15–20 % too large.

In addition, so-called longitudinal second-harmonic and subsequent sum-frequency generation can also contribute to the third-order nonlinearity: if we illuminate, e.g., a *c* plate of $KNbO_3$ with an *a*-polarized fundamental beam, a longitudinal polarization can be generated through the nonlinear optical susceptibility $\chi^{(2)}_{311}$. The associated field cannot

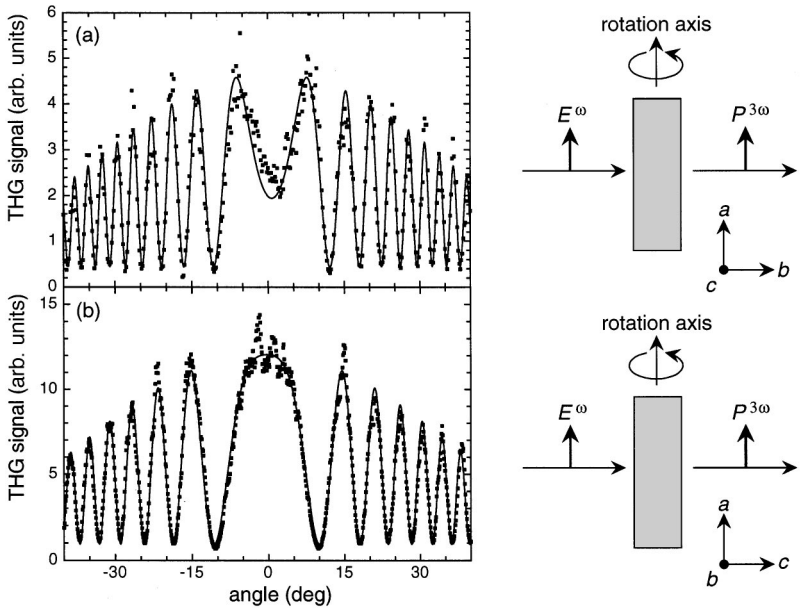

FIG. 8. Third-harmonic Maker-fringe curves of $KNbO_3$ at $\lambda = 1907$ nm to determine $\chi^{(3)}_{1111}$. (a) *b* plate with light polarizations along *a*. Cascaded contributions are present but not visible due to an unfavorable combination of coherence lengths. (b) *c* plate with light polarizations along *a* where cascaded second-order contributions can be neglected.

propagate, but can couple to the field at frequency ω through $\chi^{(2)}_{131}$, and can also contribute to the signal at frequency 3ω. Therefore, in contrast to the cases above, no additional interference effects appear in the third-harmonic Maker-fringe curves [Fig. 8(b)]. Since the contribution from longitudinal cascading is small in our case, the experiments for the *c* plate therefore directly yield $\chi^{(3)}_{1111}$ and $\chi^{(3)}_{2222}$ (Table IV).

We have seen above that in the case of α-quartz the second-order effects are dominated by the third-order ones, leading to a considerable uncertainty in the determination of the ratio $\chi^{(3)}_{1111}/[\chi^{(2)}_{111}]^2$. The other extreme case in which the combination of cascaded second-harmonic and sum-frequency generation completely dominates direct third-harmonic generation was observed for the case of the organic crystal DAST, where we performed experiments with *b* and *c* plates. At $\lambda = 2100$ nm, $\chi^{(3)}_{1111}$ could not be determined since the product $\chi^{(2)}_{111}(-3\omega,2\omega,\omega)\times\chi^{(2)}_{111}(-2\omega,\omega,\omega)$ is too large (Fig. 9): $\chi^{(3)}_{1111}$ could be varied from 0 to 5000 times $\chi^{(3)}_{fs}$ in the theoretical analysis (see the Appendix), without significantly changing the experimental Maker-fringe curves.

C. Third-harmonic generation in centrosymmetric materials

$KTaO_3$ only has the two independent components $\chi^{(3)}_{1111} = \chi^{(3)}_{2222} = \chi^{(3)}_{3333}$ and $\chi^{(3)}_{2233} = \chi^{(3)}_{1133} = \cdots$. These two components can be determined through two independent measurements, e.g., by measuring the third-harmonic signal for light propagation along the crystallographic *b* direction both for light polarized (i) along the crystallographic *a* axis for $\chi^{(3)}_{1111}(-3\omega,\omega,\omega,\omega)$ as well as (ii) at 45° to this direction for $\chi^{(3)}_{\text{eff}} = 0.5[\chi^{(3)}_{1111} + 3\chi^{(3)}_{1133}]$ (polarization and rotation axis always parallel to each other; see Table IV).

In isotropic glasses all tensor elements are equal. Figure 10 show an example of experimental curves for fused silica, BK7, and SF59.

VI. DISCUSSION AND CONCLUSIONS

A. Absolute value of the third-order susceptibilities and evaluation of reference materials

We have determined a reliable standard value for fused silica for several wavelengths based on third-harmonic-generation measurements using cascaded second-harmonic and sum-frequency generation. The use of $KNbO_3$ leads to a more precise determination, since its second-order susceptibilities are much larger than the ones of α-quartz and we therefore obtain more favorable ratios $\chi^{(3)}/[\chi^{(2)}]^2$. The required second-order susceptibility $\chi^{(2)}_{333}$ determined in this work are larger than the ones in a recently published paper.[36] We speculate that the sample used in that work might have been of inferior quality.

At $\lambda = 1907$ nm we can compare our results to other experiments. Our reference value for fused silica of $\chi^{(3)} = (1.62 \pm 0.06)\times 10^{-22}$ m^2/V^2, derived from our experi-

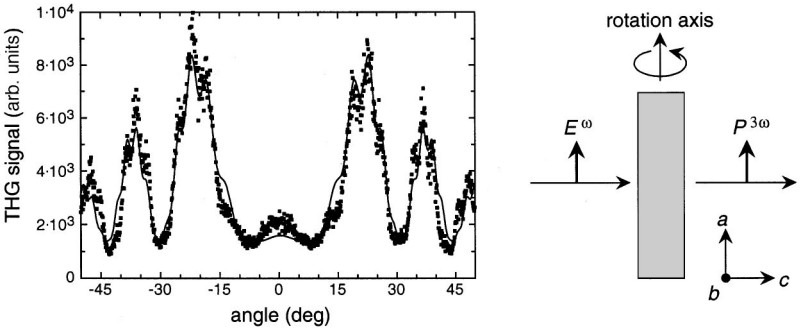

FIG. 9. Third-harmonic Maker-fringe curve of a *c* plate of DAST at $\lambda = 2100$ nm for light polarizations along *a* where cascaded second-order contributions appear. The theoretical analysis gave

$$\text{sqrt}[\chi^{(2)}_{111}(-3\omega,2\omega,\omega)\times\chi^{(2)}_{111}(-2\omega,\omega,\omega)] = 520 \text{ pm/V},$$

in good agreement with expected values based on measured nonlinear optical coefficients of DAST.

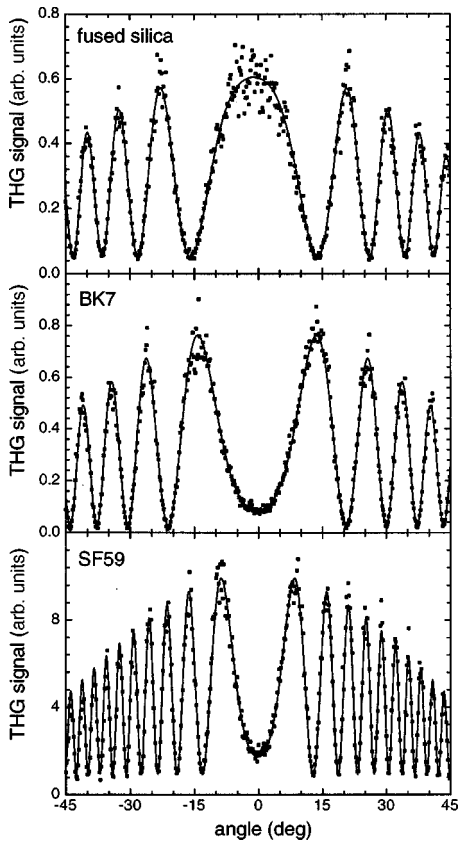

FIG. 10. Examples of third-harmonic Maker-fringe curves of fused silica, BK7 and SF59, at $\lambda = 2100$ nm.

ments, is a factor of 2.40 lower than the one currently used $[\chi^{(3)} = (3.89 \pm 0.15) \times 10^{-22}\ \mathrm{m^2/V^2}]$.[12] By adjusting the reference value for $\chi^{(2)}_{111}$ of α-quartz in Ref. 12 to the same one used here, we obtain a nonlinear optical susceptibility which is a factor of 2.46 smaller than the value in that reference, which is in excellent agreement with the factor of 2.40 mentioned above. For α-quartz we obtain a smaller ratio of $R_1 = \chi^{(3)}_{1111}/[\chi^{(2)}_{111}]^2 = 602$ than Meredith did in Ref. 12 ($R_1 = 668$). On the other hand, we obtained a larger value for $R_2 = \chi^{(3)}_{fs}/\chi^{(3)}_{1111} = 0.814 \pm 0.018$ compared to $R_2 = 0.732$.[37] The product $R_1 \times R_2$ gives the same value in both cases. On the other hand, we measured $\chi^{(3)}_{fs}/\chi^{(3)}_{3333} = 0.764 \pm 0.029$, and might therefore speculate that the y and z axes in the α-quartz sample used in Ref. 37 were interchanged by error.

In a more recent work, Mito, Hagimote, and Takahashi also carried out experiments with α-quartz at the same wavelength.[4] They obtained $\chi^{(3)}_{fs} = (1.33 \pm 0.15) \times 10^{-22}\ \mathrm{m^2/V}$. The discrepancy with our data is mainly due to a different ratio of $\chi^{(3)}_{fs}/\chi^{(3)}_{1111}$, for which they obtained 0.732 ± 0.022.

Our procedure, based on gas-phase third-harmonic-generation experiments of fused silica, gave an excellent agreement with the results presented here.[38] Specifically we obtained $\chi^{(3)}_{fs} = (2.0 \pm 0.2) \times 10^{-22}\ \mathrm{m^2/V}$ at $\lambda = 1064$ nm and $\chi^{(3)}_{fs} = (1.6 \pm 0.2) \times 10^{-22}\ \mathrm{m^2/V}$ at $\lambda = 1907$ nm in those experiments (see Ref. 38, this issue). In comparison to previously published values of BK7, we find slightly lower values for BK7 $[\chi^{(3)} = (1.47 \pm 0.07) \times \chi^{(3)}_{fs}$ as compared to $\chi^{(3)} = 1.67 \times \chi^{(3)}_{fs}$ at $\lambda = 1907$ nm].[37]

The silicate glass SF59 has a third-order nonlinearity that is about 25 times as large as fused silica (Table IV). Although less nonlinear than, e.g., $KTaO_3$, it is well suited as a reference material since (i) the nonlinearity is much larger than the one of fused silica, and (ii) it is a glass that can easily be cut and polished, that is, it combines sufficiently high third-order nonlinearities with excellent optical quality. We therefore propose the silicate glass SF59 as one of the best reference materials for the determination of third-order susceptibilities.

Based on measured second-order hyperpolarizabilities in solution the macroscopic third-order nonlinearities of DAST were estimated using the oriented gas model.[39] We calculated extremely large values ($\chi^{(3)}_{1111} > 8000 \times \chi^{(3)}_{fs}$) due to the high degree of orientation and the large packing density of the molecules in the crystal lattice in comparison to disordered polymers. Unfortunately our preliminary results showed that the cascaded contributions completely mask the third-order nonlinearity. $\chi^{(3)}_{1111}$ could be varied from 0 to $5000 \times \chi^{(3)}_{fs}$ in the theoretical analysis without significantly changing the experimental Maker-fringe curves. This finding sets an upper limit of $\chi^{(3)}_{1111} < 5000 \times \chi^{(3)}_{fs}$.

B. Boundary conditions

We analyzed the influence of the boundary conditions on the measured third-order susceptibility $\chi^{(3)}$. As can be seen from Tables III and IV, the influence of the transverse boundary conditions was up to 10% for the crystals investigated ($\leqslant$10% change of $\chi^{(3)}$ with and without this contribution for $KNbO_3$, and no change for α-quartz). The boundary conditions did not influence our results on the absolute values of fused silica.

In the case of longitudinal contributions (e.g., frequency doubling using $\chi^{(2)}_{311}$ for perpendicular incidence on a c plate of $KNbO_3$, with light polarized along a in combination with sum-frequency generation based on $\chi^{(2)}_{131}$), our estimations showed that the longitudinal field generated at frequency 2ω leads to an increase in the third-order susceptibility of $KNbO_3$ of at most 2% (and is within experimental error). If we also include the longitudinal boundary conditions this increase is almost exactly compensated for. These observations are understandable from looking at Eqs. (15) and (17): the factor $1/(n^{2\omega})^2$ is considerably smaller than $1/[(n^{\omega})^2 - (n^{2\omega})^2]$, which explains the small contribution of longitudinal cascading to $\chi^{(3)}$. Second, the ratios $1/(n^{2\omega})^2$ and $1/[(n^{\omega})^2 + (n^{2\omega})^2]$ in Eq. (17) do not differ very much, which explains the compensation of the two terms.

DAST, with its huge second-order susceptibilities, was hoped to be more susceptible to the boundary conditions. Unfortunately, we could not detect any remarkable effects either. Nevertheless organic crystals may be the best solution to obtain a unequivocal interpretation of the importance of the boundary conditions: If intermolecular interactions between the molecules in the crystal lattice can be neglected, a combination of measurements with different input polarizations and crystal plates may yield reliable quantitative results.

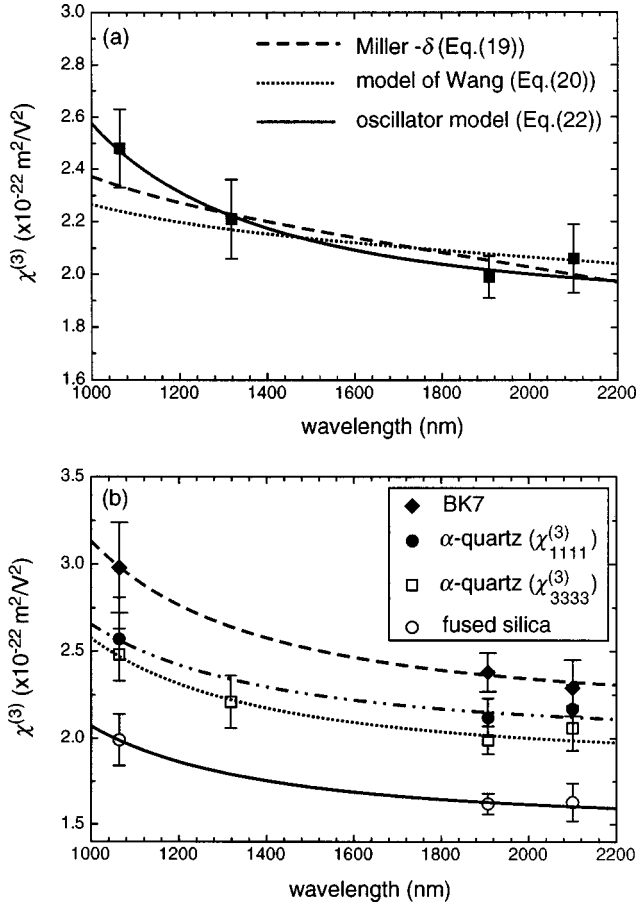

FIG. 11. (a) Comparison of different models for the description of the wavelength dispersion of $\chi^{(3)}_{1111}$ of α-quartz. The single-oscillator model best represents the experimental data points. (b) Wavelength dispersion of the third-order susceptibilities of fused silica, α-quartz, and BK7. The theoretical curves are based on the oscillator model [Eq. (22)].

C. Dispersion of the third-order susceptibilities

Figure 11 shows the dispersion of the third-order nonlinear optical susceptibilities of fused silica, α-quartz, and BK7. Figure 11(b) displays the different dispersion functions for the case of $\chi^{(3)}_{1111}$. We can clearly see that the oscillator model in Eq. (22) gives the best agreement with the experimental data. In Fig. 11(b) all three materials and the corresponding theoretical curves are displayed. The associated parameters are listed in Table V.

TABLE V. Parameters describing the dispersion of the third-order susceptibilities based on the single-oscillator model.

Material	$\delta_{1111}\times\varepsilon_0$ (10^8 m^2 s^8/V^2)	λ_0 (nm)
fused silica	6.600	156.5
α-quartz ($\chi^{(3)}_{1111}$)	7.744	157.6
α-quartz ($\chi^{(3)}_{3333}$)	14.097	147.6
BK7	5.422	167.8

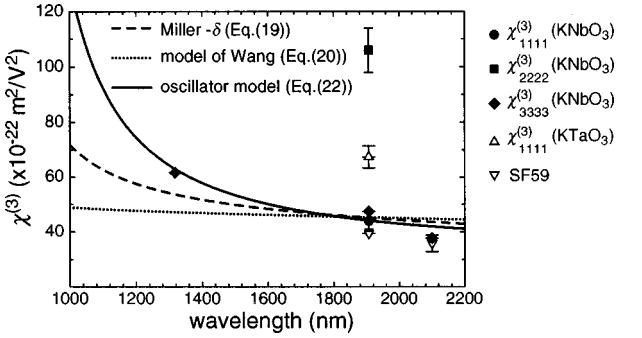

FIG. 12. Wavelength dispersion of the third-order susceptibilities of $KNbO_3$, $KTaO_3$, and SF59. The single-oscillator model best represents the experimental data points for $\chi^{(3)}_{3333}$ of $KNbO_3$.

For the cases of $KNbO_3$, $KTaO_3$, and SF59, we do not have enough data points to theoretically describe the wavelength dispersion of the third-order nonlinear optical susceptibility. We can still illustrate, however, that the harmonic-oscillator model would yield the most useful description for $KNbO_3$ (Fig. 12). As in the case of $\chi^{(2)}_{333}$, however, an infrared contribution has to be taken into account. To include this contribution in the wavelength dependence more data points are needed.

D. Structure-property relationships

Since $KNbO_3$ is cubic at high temperatures we can compare the electronic nonlinearities of the two perovskites $KNbO_3$ and $KTaO_3$ under the assumptions that the cubic (pure $\chi^{(3)}$) contributions to the third-order nonlinearities are equal, and that the temperature dependence of $\chi^{(3)}$ can be neglected. In this case the cubic nonlinear optical susceptibilities of $KNbO_3$ can be calculated from the ones of $KTaO_3$ by a rotation of 45° of the $\chi^{(3)}$ tensor around the b axis. We then theoretically obtain $\chi^{(3)}_{1111}(KNbO_3)=\chi^{(3)}_{3333}(KNbO_3)=\chi^{(3)}_{\rm eff}(KTaO_3)$ and $\chi^{(3)}_{2222}(KNbO_3)=\chi^{(3)}_{3333}(KTaO_3)$. Our experiments yielded an excellent correspondence of $\chi^{(3)}_{3333}$ and $\chi^{(3)}_{1111}(KNbO_3)$ with $\chi^{(3)}_{\rm eff}(KTaO_3)$ (Table IV). This indicates similar bond nonlinearities in these two compounds.[40] For $\chi^{(3)}_{2222}(KNbO_3)$, the simple model breaks down. The fact that $\chi^{(3)}_{2222}(KNbO_3)>\chi^{(3)}_{3333}(KTaO_3)$ is reasonable, however, since the lattice constant of $KNbO_3$ along b is considerably smaller than along a and c. Note that the b axis of $KNbO_3$ is also the direction along which we have the largest linear refractive index.

E. Third-harmonic generation vs degenerate four-wave mixing

Based on our dispersion relation for the third-order susceptibility of fused silica, we can estimate the electronic contribution to the nonlinear refractive index n_2 that is relevant for all-optical signal processing applications and which is defined through

$$n=n_0+n_2I \tag{25}$$

where I is the light intensity. n_2 and $\chi^{(3)}$ are related through

$$n_2 = \frac{3\,\mathrm{Re}[\chi^{(3)}(-\omega,\omega,-\omega,\omega)]}{4n_0^2 c\varepsilon_0}, \tag{26}$$

with c the velocity of light in vacuum. The modification of Eq. (22) for four-wave-mixing yields

$$\chi^{(3)}_{iiii}(-\omega,\omega,-\omega,\omega) = \varepsilon_0 \frac{\delta_{iiii}}{(\omega_0^2-\omega^2)^4}. \tag{27}$$

If we take the parameters of Table V, insert them into Eq. (27), and use Eq. (26), we obtain a value for n_2 of fused silica of $(2.2\pm0.1)\times10^{-20}$ m^2/W at $\lambda=1064$ nm. If we compare this value with the generally accepted one of $n_2=(2.74\pm0.17)\times10^{-20}$ m^2/W,[41] we obtain a good agreement. Moreover, we can conclude that most of the nonlinearity of fused silica in the degenerate case of equal interacting frequencies is electronic in nature.

For SF59 we cannot provide a dispersion relation, since not enough data points are available. Nevertheless, in first approximation we can compare the measured ratios of $\chi^{(3)}(-3\omega,\omega,\omega,\omega)/\chi^{(3)}_{fs}(-3\omega,\omega,\omega,\omega)$, determined here with the measured ratios of

$$\chi^{(3)}(-\omega,\omega,-\omega,\omega)/\chi^{(3)}_{fs}(-\omega,\omega,-\omega,\omega),$$

determined by the z-scan technique[20] in our laboratory. This comparison gives 24.8 (measured by third-harmonic generation at $\lambda=1907$ nm) with respect to 23.0 (measured with the z-scan technique at $\lambda=1064$ nm). Since all measurements were performed away from electronic resonances, we can again conclude that the contribution to $\chi^{(3)}(-\omega,\omega,-\omega,\omega)$ is mostly of electronic origin.

Third-order susceptibilities $\chi^{(3)}(-\omega,\omega,-\omega,\omega)$ of $KNbO_3$ were determined with degenerate four-wave mixing with 100-ps pulses at $\lambda=1064$ nm.[8] A ratio of $\chi^{(3)}_{2222}/\chi^{(3)}_{3333}=180/60=3.0$ was obtained. If we compare these results with third-harmonic generation, $\chi^{(3)}_{2222}/\chi^{(3)}_{3333}=106/47.4=2.2\pm0.2$, we also find a strong anisotropy. The difference between the two ratios results likely from additional contributions from optical phonons in the former case, since they also play an important role for the dielectric constant and the linear electro-optic effect.[42] Our findings are further supported by the fact that $\chi^{(3)}(-\omega,\omega,-\omega,\omega) > \chi^{(3)}(-3\omega,\omega,\omega,\omega)$ for both tensor elements.

Finally we can look at $KTaO_3$. Third-harmonic generation yields a ratio of $\chi^{(3)}(-3\omega,\omega,\omega,\omega)/\chi^{(3)}_{fs}(-3\omega,\omega,\omega,\omega)=41$, whereas the z-scan technique gives $\chi^{(3)}(-\omega,\omega,-\omega,\omega)/\chi^{(3)}_{fs}(-\omega,\omega,-\omega,\omega)=80$. This again implies stronger contributions to $\chi^{(3)}(-\omega,\omega,-\omega,\omega)$ from optical phonons, since both measurements were carried out far away from electronic resonances.

We can also compare the third-order susceptibility of fused silica with those of α-quartz. Both materials are made out of the same atoms (Si, O_2). We could therefore expect to have the same values which is obviously not the case [e.g., $\chi^{(3)}{}_{1111}(\alpha\text{-quartz})/\chi^{(3)}(\text{fused silica})=1.26$]. We can first apply the Miller δ [Eq. (19)], which should be adequate for a comparison at identical wavelengths, and we therefore expect the same value for the Miller δ. If we compare the values at, e.g., $\lambda=2100$ nm, we obtain $\delta_{1111}(\alpha\,\text{quartz})/\delta(\text{fused silica})=0.55$ and $\delta_{3333}(\alpha\text{-quartz})/\delta(\text{fused silica})=0.54$: the ratio becomes worse. However, we did not take the density ρ adequately into account.[37] According to the Clausius-Mossotti equation the density is proportional to $(n^2-1)/(n^2+1)$, and therefore the Miller δ is proportional to ρ^{-4}. To correct for this fact it should be more appropriate to use a modified Miller δ given by $\delta'=\delta\times\rho^3$. We then obtain the following relations: $\delta'_{1111}(\alpha\text{-quartz})/\delta(\text{fused silica})=0.96$ and $\delta'_{3333}(\alpha\text{-quartz})/\delta(\text{fused silica})=0.94$. The agreement between fused silica and α-quartz is much improved, and we see that the density correction is necessary.

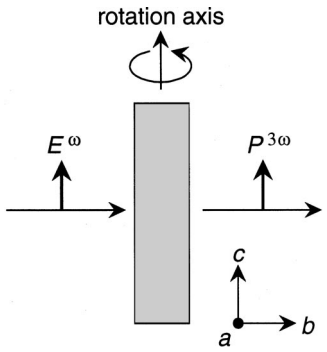

FIG. 13. Schematic of the experimental sample geometry for the case of s-polarized beams corresponding to the measurement of $\chi^{(3)}_{3333}$ of a $KNbO_3$ crystal in air.

F. Conclusions

Third-harmonic generation provides a direct measurement of the purely electronic third-order nonlinear optical response. This is an advantage with respect to most other techniques that measure a combination of electronic and other distortional effects that are often difficult or even impossible to resolve. We have determined new reliable reference values for the electronic third-order susceptibilities $\chi^{(3)}(-3\omega,\omega,\omega,\omega)$ [e.g., $\chi^{(3)}_{fs}=(1.62\pm0.06)\times10^{-22}$ m^2/V^2 at $\lambda=1907$ nm] due to the combination of second-and third-harmonic generation exploiting cascaded second-order nonlinearities using α-quartz and $KNbO_3$. We analyzed the boundary conditions relevant in third-harmonic generation of noncentrosymmetric materials, and showed that in the case of the high nonlinearity materials $KNbO_3$ and DAST its influence on the measured values was up to 10%. We demonstrated that a simple oscillator model adequately describes the wavelength dispersion of the third-order susceptibility in the measured wavelength range. We suggest the silicate glass SF59 as a suitable candidate for a reference material at the moment. The different measured values of fused silica and α-quartz could be interpreted by taking into account the different densities. For the case of $KNbO_3$, we found considerable anisotropies in third-harmonic generation and degenerate four-wave mixing. The difference in these anisotropies is attributed to additional optical-phonon contributions in the latter case. Using a simple model we could nicely correlate the third-order nonlinearities of $KNbO_3$ and $KTaO_3$. This indicates similar bond nonlinearities in these two compounds.

APPENDIX: THEORETICAL DESCRIPTION OF THIRD-HARMONIC GENERATION IN SINGLE CRYSTALS INCLUDING CASCADED SECOND-ORDER CONTRIBUTIONS

We assume that the fundamental, the second-harmonic (in the case of cascading), and the third-harmonic waves are all *s* polarized (e.g., along the *c* axis in the case of $\chi^{(3)}_{3333}$ of $KNbO_3$), and that the sample is rotated around the same axis (Fig. 13). The nonlinear optical susceptibilities are defined as in Eqs. (4)–(6), where $\chi^{(2)}(\chi^{(2)'})$ represents the process of frequency doubling (sum-frequency generation). By solving the wave equation and applying the electromagnetic boundary conditions, the field at the third harmonic can be calculated. The theory described here extends the work of Ref. 12 to rotational Maker-fringe curves. In comparison to Ref. 4 we explicitly include contributions from air.

The calculations yield the total field at frequency 3ω after the sample

$$\begin{aligned}|E_{\mathrm{tot}}|^2 = {} & C_{\mathrm{dir}} + (E_{b1}-E_{b2})^2 + (E'_{b1}-E'_{b2})^2 + 2(E'_{b1}-E'_{b2}) \\ & \times (E_{b1}-E_{b2}) + 4E_{b1}[E_{b2}+E'_{b2}]\sin^2\left(\frac{\Delta k^{3\omega}L}{2}\right) \\ & + 4E'_{b1}[E_{b2}+E'_{b2}]\sin^2\left(\frac{\Delta k^{321\omega}L}{2}\right) \\ & - 4E_{b1}E'_{b1}\sin^2\left(\frac{\Delta k^{3\omega'}L}{2}\right). \end{aligned} \tag{A1}$$

The different quantities are described in the following. The index *b* always denotes bound wave. The contribution from air is contained in

$$\begin{aligned} C_{\mathrm{air}} = {} & (E_{\mathrm{air\_1}}-E_{\mathrm{air\_2}})^2 - 2(E_{\mathrm{air\_1}}-E_{\mathrm{air\_2}})(E_{b2}+E'_{b2}) \\ & + 2(E_{b1}+E'_{b1})(E_{\mathrm{air\_1}}-E_{\mathrm{air\_2}}) - 4\sin^2\left(\frac{\Delta k^{3\omega}L}{2}\right) \\ & \times [E_{b1}E_{\mathrm{air\_1}} + E_{b2}E_{\mathrm{air\_2}} + E'_{b2}E_{\mathrm{air\_2}} - E_{\mathrm{air\_1}}E_{\mathrm{air\_2}}] \\ & - 4\sin^2\left(\frac{\Delta k^{321\omega}L}{2}\right)E'_{b1}E_{\mathrm{air\_1}} \\ & + 4\sin^2\left(\frac{\Delta k^{3\omega'}L}{2}\right)E'_{b1}E_{\mathrm{air\_2}}. \end{aligned} \tag{A2}$$

The wave vector mismatches are given by

$$\begin{aligned} \Delta k^{3\omega} &= k_b^{3\omega}\cos\theta^{\omega} - k^{3\omega}\cos\theta^{3\omega} \\ &= \frac{6\pi}{\lambda}(n^{\omega}\cos\theta^{\omega} - n^{3\omega}\cos\theta^{3\omega}), \end{aligned}$$

$$\begin{aligned} \Delta k^{3\omega'} &= k_b^{3\omega}\cos\theta^{\omega} - k^{2\omega}\cos\theta^{2\omega} - k^{\omega}\cos\theta^{\omega} \\ &= \frac{4\pi}{\lambda}(n^{\omega}\cos\theta^{\omega} - n^{2\omega}\cos\theta^{2\omega}), \end{aligned} \tag{A3}$$

$$\begin{aligned} \Delta k^{321\omega} &= k^{3\omega}\cos\theta^{3\omega} - k^{2\omega}\cos\theta^{2\omega} - k^{\omega}\cos\theta^{\omega} \\ &= \frac{2\pi}{\lambda}(3n^{3\omega}\cos\theta^{3\omega} - 2n^{2\omega}\cos\theta^{2\omega} - n^{\omega}\cos\theta^{\omega}), \end{aligned}$$

where n is the refractive index of the sample, L is the sample thickness, and $\theta^{\omega}(\theta^{2\omega},\theta^{3\omega})$ is the internal angle of incidence of the wave at the appropriate frequency. The further quantities are

$$E_{\mathrm{air\_1}} = t^{3\omega}_{0/1}t^{3\omega}_{1/2}\chi^{(3)}_{\mathrm{air}} \quad E_{\mathrm{air\_2}} = (t^{\omega}_{0/1}t^{\omega}_{1/2})^3\chi^{(3)}_{\mathrm{air}}, \tag{A4}$$

$$E_{b1} = T_1^{1/2}E_b^{3\omega}, \quad E_{b2} = t^{3\omega}_{1/2}T_2^{0/1}E_b^{3\omega}, \tag{A5}$$

$$E'_{b1} = (T_1^{1/2})'E_b^{3\omega'}, \quad E'_{b2} = t^{3\omega}_{1/2}(T_2^{0/1})'E_b^{3\omega'}. \tag{A6}$$

In the case of cascading induced by transverse waves at the second-harmonic frequency, we have (where E^{ω} is the external field at frequency ω)

$$\begin{aligned} E_b^{3\omega} = {} & (t^{\omega}_{0/1})^3\frac{1}{(n^{\omega})^2-(n^{3\omega})^2}\left(\frac{1}{4}\chi^{(3)} + \frac{1}{2}\chi^{(2)}(\chi^{(2)})'\right. \\ & \left.\times\frac{1}{(n^{\omega})^2-(n^{2\omega})^2} + \frac{1}{2}\chi^{(2)}(\chi^{(2)})'\varepsilon_0\frac{L^{2\omega}}{f^{2\omega}}\right)(E^{\omega})^3. \end{aligned} \tag{A7}$$

In the case of cascading through longitudinal fields at frequency 2ω (as e.g., for a *c* plate of $KNbO_3$), we have

$$\begin{aligned} E_b^{3\omega} = {} & (t^{\omega}_{0/1})^3\frac{1}{(n^{\omega})^2-(n^{3\omega})^2}\left(\frac{1}{4}\chi^{(3)} - \frac{1}{2}\chi^{(2)}_{\mathrm{long}}(\chi^{(2)}_{\mathrm{long}})'\frac{1}{(n^{2\omega}_{\mathrm{long}})^2}\right. \\ & \left. + \frac{1}{2}\chi^{(2)}_{\mathrm{long}}(\chi^{(2)}_{\mathrm{long}})'\varepsilon_0\frac{L^{2\omega}}{f^{2\omega}_{\mathrm{long}}}\right)(E^{\omega})^3. \end{aligned} \tag{A8}$$

Here $\chi^{(2)}_{\mathrm{long}}$ represents the second harmonic that is generated along the propagation direction of the fundamental (e.g., $\chi^{(2)}_{311}$ for perpendicular incidence on a *c* plate of $KNbO_3$ with light polarized along *a*). Note that in this case the field generated at 2ω does not propagate itself. Likewise n_{long} is the refractive index along the propagation direction. Local-field corrections are accounted for through

$$L = \frac{1}{3\varepsilon_0}, \quad f^{2\omega} = \frac{(n^{2\omega})^2+2}{3}, \quad f^{2\omega}_{\mathrm{long}} = \frac{(n^{2\omega}_{\mathrm{long}})^2+2}{3}. \tag{A9}$$

$E_b^{3\omega'}$ is given by

$$E_b^{3\omega'} = -(t^{\omega}_{0/1})^3\frac{9}{(n^{\omega})^2+4(n^{2\omega})^2+4n^{\omega}n^{2\omega}\cos(\theta^{2\omega}-\theta^{\omega})-9(n^{3\omega})^2}T_{vv}\frac{1}{2}\chi^{(2)'}\chi^{(2)}\frac{1}{(n^{\omega})^2-(n^{2\omega})^2}(E^{\omega})^3. \tag{A10}$$

The transmission factors for the fundamental and third-harmonic waves are given by (θ is the external angle of incidence)

$$t_{0/1}^{\omega}=\frac{2\cos\theta}{n^{\omega}\cos\theta^{\omega}+\cos\theta},\quad t_{1/0}^{\omega}=\frac{2n^{\omega}\cos\theta^{\omega}}{n^{\omega}\cos\theta^{\omega}+\cos\theta}, \tag{A11}$$

$$t_{0/1}^{3\omega}=\frac{2\cos\theta}{n^{3\omega}\cos\theta^{3\omega}+\cos\theta},\quad t_{1/0}^{3\omega}=\frac{2n^{3\omega}\cos\theta^{3\omega}}{n^{3\omega}\cos\theta^{3\omega}+\cos\theta}, \tag{A12}$$

The factors resulting from the electromagnetic boundary conditions at the different interfaces are expressed as

$$T_{vv}=\frac{\cos\theta+n^{\omega}\cos\theta^{\omega}}{\cos\theta+n^{2\omega}\cos\theta^{2\omega}}, \tag{A13}$$

$$T_2^{0/1}=\frac{n^{\omega}\cos\theta^{\omega}+\cos\theta}{n^{3\omega}\cos\theta^{3\omega}+\cos\theta}$$

$$(T_2^{0/1})'=\frac{\frac{1}{3}(2n^{2\omega}\cos\theta^{2\omega}+n^{\omega}\cos\theta^{\omega})+\cos\theta}{n^{3\omega}\cos\theta^{3\omega}+\cos\theta}, \tag{A14}$$

$$T_1^{1/2}=\frac{n^{3\omega}\cos\theta^{3\omega}+n^{\omega}\cos\theta^{\omega}}{n^{3\omega}\cos\theta^{3\omega}+\cos\theta}$$

$$(T_1^{1/2})'=\frac{\frac{1}{3}(2n^{2\omega}\cos\theta^{2\omega}+n^{\omega}\cos\theta^{\omega})+n^{3\omega}\cos\theta^{3\omega}}{n^{3\omega}\cos\theta^{3\omega}+\cos\theta}, \tag{A15}$$

Incoherent multiple reflections were taken into account through Eq. (24).

*Electronic address: bosshard@iqe.phys.ethz.ch

[1] R. C. Eckardt, H. Masuda, Y. X. Fan, and R. L. Byer, IEEE J. Quantum Electron. **26**, 922 (1990).
[2] D. A. Roberts, IEEE J. Quantum Electron. **28**, 2057 (1992).
[3] A. Kitamoto, T. Kondo, I. Shoji, and R. Ito, Opt. Rev. **2**, 280 (1995).
[4] A. Mito, K. Hagimoto, and C. Takahashi, Nonlinear Opt. **13**, 3 (1995).
[5] R. C. Miller, Appl. Phys. Lett. **5**, 17 (1964).
[6] T. Pliska, F. Mayer, D. Fluck, P. Günter, and D. Rytz, J. Opt. Soc. Am. B **12**, 1878 (1995).
[7] M. Zgonik and P. Günter, J. Opt. Soc. Am. B **13**, 570 (1996).
[8] I. Biaggio, Phys. Rev. Lett. **82**, 193 (1999).
[9] Ch. Bosshard, R. Spreiter, M. Zgonik, and P. Günter, Phys. Rev. Lett. **74**, 2816 (1995).
[10] J. F. Nye, *Physical Properties of Crystals* (Clarendon, Oxford, 1967).
[11] C. Flytzanis and N. Bloembergen, Prog. Quantum Electron. **4**, 271 (1976).
[12] G. R. Meredith, Phys. Rev. B **24**, 5522 (1981).
[13] L. A. Ostrovskii, JETP Lett. **5**, 272 (1967).
[14] D. N. Klyshko and B. F. Polkovnikov, Sov. J. Quantum Electron. **3**, 324 (1974).
[15] J.-M. R. Thomas and J.-P. E. Taran, Opt. Commun. **4**, 329 (1972).
[16] S. A. Akhmanov, A. I. Kovrygin, and A. P. Sukhorukov, in *Quantum Electronics: A Treatise, Nonlinear Optics* edited by H. Rabin and C. L. Tang, (Academic, New York, 1975), Vol. 1, Pt. B, p. 476.
[17] G. I. Stegeman, D. J. Hagan, and L. Torner, J. Op. Quantum. Electron **28**, 1691 (1996).
[18] T. K. Gustafson, J.-P. E. Taran, P. L. Kelley, and R. Y. Chiao, Opt. Commun. **2**, 17 (1970).
[19] Ch. Bosshard, I. Biaggio, St. Fischer, S. Follonier, and P. Günter, Opt. Lett. **24**, 196 (1999).
[20] M. Sheik-Bahae, A. A. Said, W. Tai-Huei, D. J. Hagan, and E. W. Van Stryland, IEEE J. Quantum Electron. **26**, 760 (1990).
[21] R. W. Hellwarth, Prog. Quantum Electron. **5**, 1 (1977).
[22] D. Bedeaux and N. Bloembergen, Physics **69**, 57 (1973).
[23] J. J. Wynne, Phys. Rev. **178**, 1295 (1969).
[24] C. C. Wang, Phys. Rev. B **2**, 2045 (1970).
[25] N. Boling, A. J. Glass, and A. Owyoung, IEEE J. Quantum Electron. **14**, 601 (1978).
[26] R. W. Boyd, *Nonlinear Optics* (Academic, San Diego, 1992).
[27] D. W. Hall, M. A. Newhouse, N. F. Borelli, W. H. Dumbaugh, and D. L. Weidman, Appl. Phys. Lett. **54**, 1293 (1989).
[28] S. R. Friberg and P. W. Smith, IEEE J. Quantum Electron. **23**, 2089 (1987).
[29] *Ferro-und Antiferroelektrische Substanzen*, 3rd ed. edited by K.-H. Hellwege and A. M. Hellwege, (Springer-Verlag, Heidelberg, 1969).
[30] G. Shirane, H. Danner, A. Pavlovic, and R. Pepinsky, Phys. Rev. **93**, 672 (1954).
[31] U. Meier, M. Bösch, Ch. Bosshard, F. Pan, and P. Günter, J. Appl. Phys. **83**, 3486 (1998).
[32] S. R. Marder, J. W. Perry, and C. P. Yakymyshyn, Chem. Mater. **6**, 1137 (1994).
[33] J. Jerphagnon and S. K. Kurtz, J. Appl. Phys. **41**, 1667 (1970).
[34] Ch. Bosshard, R. Spreiter, P. Günter, R. R. Tykwinski, M. Schreiber, and F. Diederich, Adv. Mater. **8**, 231 (1996).
[35] *Handbook of Chemistry and Physics*, edited by D. R. Lide, 73 (CRC Press, Boca Raton, FL, 1992).
[36] I. Shoji, T. Kondo, A. Kitamoto, M. Shirane, and R. Ito, J. Opt. Soc. Am. B **14**, 2268 (1997).
[37] B. Buchalter and G. R. Meredith, Appl. Opt. **21**, 3221 (1982).
[38] U. Gubler and Ch. Bosshard, Following paper, Phys. Rev. B **61**, 10 702 (2000).
[39] J. Zyss and J. L. Oudar, Phys. Rev. A **26**, 2028 (1982).
[40] J. G. Bergman and G. R. Crane, J. Chem. Phys. **60**, 2470 (1974).
[41] D. Milam, Appl. Opt. **37**, 546 (1998).
[42] M. Zgonik, R. Schlesser, I. Biaggio, E. Voit, J. Tscherry, and P. Günter, J. Appl. Phys. **74**, 1287 (1993).